Rankl-induced osteoclastogenesis leads to loss of mineralization in a medaka osteoporosis model

Thuy Thanh To[1], P. Eckhard Witten[2,3], Joerg Renn[1], Dipanjan Bhattacharya[1,4], Ann Huysseune[2] and Christoph Winkler[1,*]

SUMMARY

Osteoclasts are macrophage-related bone resorbing cells of hematopoietic origin. Factors that regulate osteoclastogenesis are of great interest for investigating the pathology and treatment of bone diseases such as osteoporosis. In mammals, receptor activator of NF-κB ligand (Rankl) is a regulator of osteoclast formation and activation: its misexpression causes osteoclast stimulation and osteoporotic bone loss. Here, we report an osteoporotic phenotype that is induced by overexpression of Rankl in the medaka model. We generated transgenic medaka lines that express GFP under control of the cathepsin K promoter in osteoclasts starting at 12 days post-fertilization (dpf), or Rankl together with CFP under control of a bi-directional heat-shock promoter. Using long-term confocal time-lapse imaging of double and triple transgenic larvae, we monitored in vivo formation and activation of osteoclasts, as well as their interaction with osteoblasts. Upon Rankl induction, GFP-positive osteoclasts are first observed in the intervertebral regions and then quickly migrate to the surface of mineralized neural and haemal arches, as well as to the centra of the vertebral bodies. These osteoclasts are TRAP (tartrate-resistant acid phosphatase) and cathepsin K positive, mononuclear and highly mobile with dynamically extending protrusions. They are exclusively found in tight contact with mineralized matrix. Rankl-induced osteoclast formation resulted in severe degradation of the mineralized matrix in vertebral bodies and arches. In conclusion, our in vivo imaging approach confirms a conserved role of Rankl in osteoclastogenesis in teleost fish and provides new insight into the cellular interactions during bone resorption in an animal model that is useful for genetic and chemical screening.

KEY WORDS: Medaka, Osteoblasts, Osteoclasts, Osteoporosis, Rankl, Zebrafish

INTRODUCTION

Osteoporosis and related bone diseases are a major public health concern and have increasing impact on our ageing societies (Gallagher and Sai, 2010). Present therapies aim to increase bone strength and enhance the activity of bone-forming cells (osteoblasts), e.g. through administration of intermittent doses of parathyroid hormone. Alternatively, the activity of bone-resorbing cells (osteoclasts) is also targeted by different therapeutic approaches (reviewed in Reid, 2008). Over the past 15 years, significant progress has been made in basic bone research regarding the mechanisms that underlie bone remodelling, i.e. the constant replacement of old bone matrix by newly formed bone. Several key regulators have been described to drive differentiation of osteoblasts and osteoclasts. As part of this, a variety of animal models has been established to study bone formation and skeletal remodelling under normal and pathological conditions. However, models that allow in vivo imaging of osteoclasts in living specimens have been lacking so far.

The homeostasis of bone requires an intricate balance between osteoblasts and osteoclasts that crossregulate each other's activities. Osteoblasts control formation and activity of osteoclasts through the production of regulatory factors such as receptor activator of NF-κB ligand (Rankl) and osteoprotegerin (OPG). Formation,

maturation and activity of osteoclasts are stimulated by Rankl/Rank receptor interaction and are downregulated by factors such as osteoprotegerin (Caetano-Lopes et al., 2007; Gallagher and Sai, 2010; Reid, 2008). Importantly, the concept of a 'basic multicellular unit' (BMU) responsible for bone remodelling assumes that a constantly active feedback loop between all bone cell types is required for bone homeostasis and remodelling to maintain constant turnover of bone mineralized matrix (Harada and Rodan, 2003). According to this concept, increased bone resorption also stimulates the increase in bone formation and vice versa. Understanding the regulatory networks underlying this process is instrumental for our understanding of bone remodelling and future intervention in pathological processes (Karsenty, 2008).

Osteoblasts are derived from mesenchymal progenitor cells that also give rise to other cell types, including chondrocytes, adipocytes and muscle cells (reviewed by Karsenty, 2008; Komori, 2008). Osteoclasts, however, are bone-resorbing cells derived from the monocyte/macrophage lineage of hematopoietic stem cells (Harada and Rodan, 2003; Wagner and Karsenty, 2001). They secrete cathepsin K, tartrate-resistant acid phosphatase (TRAP) and acidify the subcellular space to degrade bone matrix proteins and dissolve bone minerals.

Mouse and chicken are classical animal models for bone research. Teleost fish, such as zebrafish (*Danio rerio*) and medaka (*Oryzias latipes*), have only recently become established for use in skeletal research, despite the possibilities of combining powerful genetics with high-resolution imaging. Like mammals, teleost fish develop bones directly from mesenchymal condensations (membranous bone formation) and on cartilage scaffolds (endochondral/perichondral bone formation) (Langille and Hall, 1988). Recent findings indicate that the genetic networks controlling bone formation are highly

[1]Department of Biological Sciences and NUS Centre for Bioimaging Sciences (CBIS), National University of Singapore, Singapore 117543. [2]Biology Department, Ghent University, Belgium. [3]Skretting Aquaculture Research Centre, Norway. [4]Singapore-MIT Alliance for Research and Technology Center (SMART).

*Author for correspondence (dbswcw@nus.edu.sg)

conserved in all vertebrates, including teleosts (Flores et al., 2004; Inohaya et al., 2007; Nemoto et al., 2007; Renn et al., 2006; Yan et al., 2005). Fish models were also successfully used to identify novel mechanisms controlling bone formation that were previously unknown in mammals (Hammond and Schulte-Merker, 2009; Inohaya et al., 2010; Spoorendonk et al., 2008). At the cellular level, osteoblasts and osteoclasts of teleosts share many functional features with their counterparts in mammals (Witten and Huysseune, 2009), thus opening the possibility of imaging the dynamic behaviour of osteoblasts and osteoclasts in the almost transparent embryos and larvae.

We have previously described a transgenic medaka line that expresses fluorescent reporters under control of the *osterix* promoter in early osteoblasts (Renn and Winkler, 2009). In the present study, we describe for the first time a triple transgenic approach that we used to study the interaction of osteoclasts and osteoblasts under normal conditions, as well as upon heat-shock-induced Rankl expression. Transgenic lines such as these allow for an in vivo approach that will provide new insights into bone diseases with a major impact on human health, such as osteoporosis.

MATERIALS AND METHODS
Identification of medaka *rankl*, sequence extension and subcloning
A partial nucleotide sequence encoding Rankl was identified by BLAST search in the medaka genome (Ensemble, ultracontig 247) using the predicted Rankl amino acid sequence of *Tetraodon nigroviridis* (CAG02628) as the query. The medaka sequence included a predicted stop codon but lacked the translation start. 5′-RACE PCR (Invitrogen) was performed using primers *ranklGSP1* and *ranklGSP2* (supplementary material Table S1). The full-length coding region of medaka *Rankl* (GenBank Accession Number JN119285) was then amplified using primers *ranklUP* and *ranklDOWN*, and subcloned into pCRII (Invitrogen) and pCS2P+ after *Eco*RI digestion. Alternatively spliced *rankl* isoforms were identified by PCR using primers R0 and R4 that flank the start and stop codons of the coding sequence and cDNA from 1-month old larvae. Three primer pairs were used to confirm alternatively spliced variants: R1 and R4 for isoform *rankl1*, R2 and R4 for *rankl2*, and R3 and R4 for *rankl3* (see supplementary material Fig. S3). Protein alignments were carried out using ClustalW2 (EMBL-EBI) and hydrophobic regions were predicted using ProtScale with the Kyte-Doolittle method (ExPASy).

Generation of transgenic fish
A 3.18 kb upstream sequence of the *cathepsin K* gene (ENSORLT00000019682), including 80 nucleotides of exon 1 was amplified using the Qiagen Long Range PCR Kit with primers *ctskUP* and *ctskDOWN*, and cloned in front of membrane-bound EGFP (mEGFP) in an I-*Sce*I meganuclease vector. Plasmid DNA (20 pg) was injected into one-cell stage medaka embryos, as described previously (Rembold et al., 2006). Injected embryos with transient mEGFP expression were raised. Three out of seven analysed fish were germline positive and all data presented below refer to heterozygous offspring of founder male 2. The construct *rankl*:HSE:CFP, containing a bidirectional heat-shock promoter driving simultaneous expression of *rankl* and CFP, was created by cloning the full-length medaka *rankl* cDNA into *Bam*HI-*Xho*I sites of a vector with I-*Sce*I sites flanking a heat-shock-CFP cassette. GFP in the original plasmid (Bajoghli et al., 2004) was replaced by CFP. The construct was injected as described above. On average, 15% of injected F0 embryos showed transient mosaic CFP expression after heat shock at 1 dpf for 2 hours at 39°C. Positive embryos were raised and three out of seven analysed F0 fish were germline positive. For all experiments described below, heterozygous offspring of female founder 4 were used as they showed highest CFP levels. Heat-shock was applied at 9 dpf or at 21 and 23 dpf for 2 hours at 39°C and mineralization was analysed at 16 dpf and 31 dpf, respectively. All experiments were performed in accordance with IACUC protocols of NUS (approval numbers 020/08, 014/11).

Cryosectioning, in situ hybridization and histochemical staining
Embryos were fixed overnight in 4% PFA, rinsed with PBST and embedded in 1.5% agarose/5% sucrose. Blocks were soaked in 30% sucrose overnight at 4°C before preparing cryosections of 20-30 μm. RNA in situ hybridizations were carried out as described (Renn et al., 2006). The full-length open reading frame of medaka *cathepsin K* (ESTs: AM149366, BJ714293, BJ880292) was amplified with primers *ctskriboUP* and *ctskriboDOWN*, cloned into pCRII (Invitrogen) and antisense riboprobes were prepared by *Xba*I digestion and Sp6 in vitro transcription. *rank* and *col1a1* were amplified with primers listed in supplementary material Table S1.

Mineralized matrix in fixed embryos was visualized with Alizarin Red (Renn and Winkler, 2009). For live staining, larvae were incubated in 0.01% alizarin-3-methyliminodiacetic acid (Alizarin Complexone; Sigma A3882) in embryo medium at 30°C for 2 hours for hatchlings and 4 hours for 3- to 4-week-old fish. After incubation, larvae were rinsed in embryo medium 2 hours to overnight before imaging. TRAP staining for whole-mount embryos and cryosections was performed using the acid phosphatase, leukocyte (TRAP) Kit (Sigma 387A) following manufacturer's recommendations. Nuclei were stained with DRAQ5 (Biostatus) diluted 1 to 250 in H_2O and applied to cryosections of larvae for 1 hour at 37°C.

Confocal and DSLM imaging
Embryos were anaesthetized with 0.1% ethyl 3-aminobenzoate methanesulfonate (Tricaine; Sigma E10521) and embedded in 1.5% low melting agarose in a glass bottom petri dish. Confocal pictures and time-lapse confocal imaging were carried out with Zeiss LSM 510 Meta and LSM 5 live microscopes using 488, 543, 633 nm laser lines for GFP, mCherry and far-red fluorophore (DRAQ5), respectively. Imaging data were processed using Imaris 7.1.1 (bitplane) and ImageJ software. For digitally scanned laser sheet microscopy (DSLM), 488nm and 561 nm lasers were used for excitation of EGFP, calcein, mCherry and Alizarin Complexone. An Olympus 4× 0.16 NA excitation objective was used for creating a laser sheet and a Zeiss, 10×, 0.3 NA water immersion objective for fluorescent collection at 28°C.

RESULTS
An osteoclast reporter line in medaka
We generated an osteoclast reporter line expressing membrane-bound EGFP (mEGFP) under control of a 3.18 kb cathepsin K (*ctsk*) promoter fragment (Fig. 1A). This line shows expression comparable with the *CTSK*-GFP line reported recently in a study that used a slightly shorter promoter (Chatani et al., 2011). Stable *ctsk*:mEGFP transgenic embryos first showed GFP expression at 5 dpf in head and tail regions (Fig. 1B-E), which did not exhibit TRAP activities at later stages (data not shown). *ctsk*:mEGFP expression recapitulated most aspects of endogenous *cathepsin K* expression revealed by RNA in situ hybridization (Fig. 1F-K). Notable exceptions were the heart, single neurons in the brain and the pineal gland that expressed *ctsk* endogenously but not in the transgenics (compare Fig. 1C,D with 1F,G). Histological analysis revealed other domains at 5 dpf with both *ctsk*:mEGFP and *cathepsin K* expression. This included the pre-muscular head mesenchyme, which later develops into, for example, the sternohyoideus muscle, and is positioned between *ctsk*-negative branchial arches and superficial epidermis (Fig. 1C,D,F,G; and data not shown), and parts of the caudal and pectoral fins (Fig. 1E,H,K). Around hatching at 12 dpf, *ctsk*:mEGFP was also found in the pharyngeal teeth area where TRAP activity was evident (Fig. 1L,M). At 3 to 4 weeks, *ctsk*:mEGFP was found in the vertebral column (Fig. 2A,B). Confocal imaging after staining with Alizarin Complexone revealed mEGFP expression around the mineralized bone matrix of neural and haemal arches, but not at the neural and haemal spines and not at the vertebral centra (Fig. 2C,D,G).
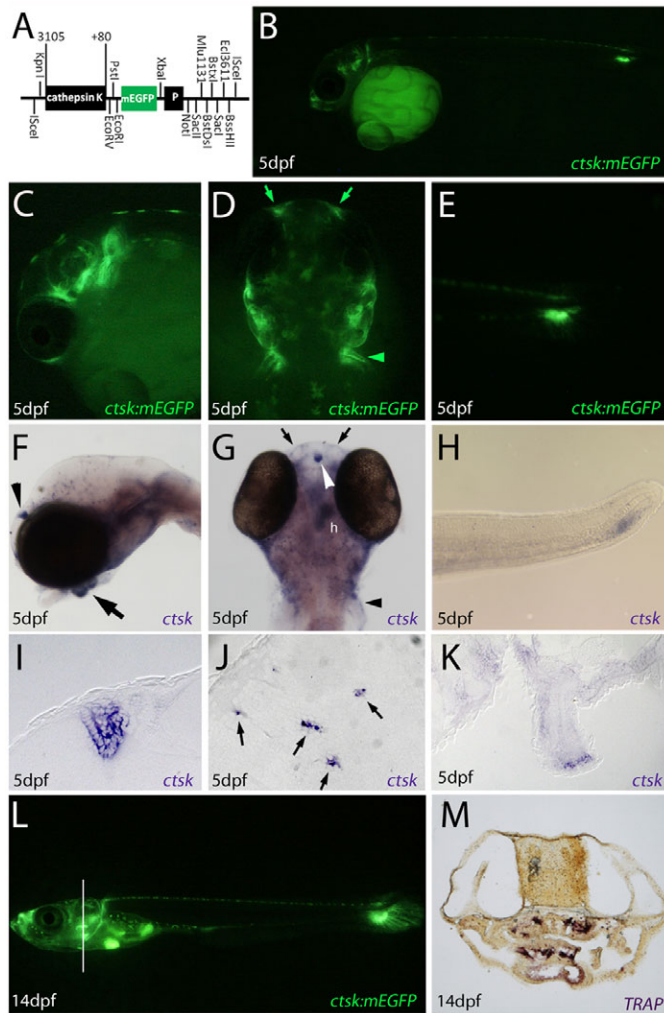
Fig. 1. Transgenic medaka expressing mEGFP under control of the *ctsk* promoter. (**A**) *ctsk*:mEGFP construct used to generate transgenic fish. P, polyadenylation signal. (**B**) *ctsk*:mEGFP expression in stable transgenic medaka at 5 dpf, lateral view. (**C-E**) Higher magnification views of head and tail regions of embryo in B (C,E, lateral; D, dorsal). Arrows in D indicate olfactory pits, arrowhead indicates fin mesenchyme. (**F-H**) Endogenous *cathepsin K* expression revealed by RNA in situ hybridization (F,H, lateral; G, dorsal; arrowheads, pineal gland; black arrowheads in G, fin mesenchyme; arrow in F, heart (h); arrows in G, olfactory pits. (**I-K**) Sagittal sections of embryo at 5 dpf showing staining in the pineal gland (I), neurons in the brain (J, arrows) and in distal rim mesenchyme of the pectoral fin (K). (**L**) *ctsk*:mEGFP expression at hatching stage (12 dpf); signal in ventral region is from autofluorescent pigment cells (see supplementary material Fig. S1). (**M**) Transverse section at level indicated in I, showing TRAP activity (red) in pharyngeal tooth region.

Histochemical analysis revealed that all GFP-expressing cells in the vertebral column are TRAP positive (Fig. 2E,F), suggesting that they are functional osteoclasts. In addition, most *ctsk*:mEGFP cells are tightly associated with osteoblasts (33 out of 39 osteoclasts analysed in seven embryos; supplementary material Movie 5). Presence of osteoclasts in this region is consistent with ongoing bone remodelling during reshaping of neural and haemal arches, creating space for the growing spinal cord and dorsal blood vessel, respectively (Witten et al., 2001). In addition, GFP expression was found at the base of the dorsal, pectoral and anal fins, and at the
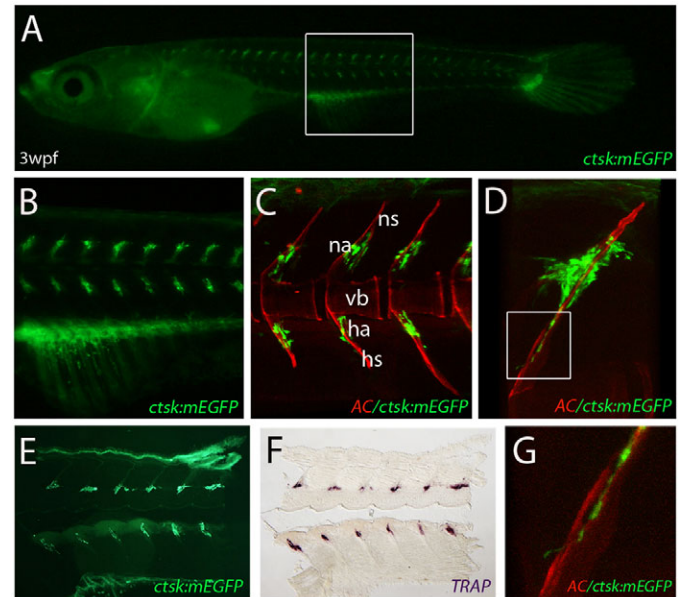

Fig. 2. Expression of *ctsk*:mEGFP in osteoclasts. (**A**) *ctsk*:mEGFP expression in the vertebral column at 3 weeks post-fertilization (wpf). (**B**) Higher magnification view of area boxed in A showing expression in the vertebral column and at the base of the anal fin. (**C**) Confocal stack of a vertebral column region at 3 wpf. Mineralized matrix is stained with Alizarin Complexone (vb, vertebral body; na, neural arch; ha, haemal arch; ns, neural spine; hs, haemal spine). (**D**) Higher magnification view of neural arch with osteoclasts (green) in cell clusters, surrounding the forming arch. (**G**) The base of the arch (boxed in D) shown at higher magnification. (**E,F**) Same sagittal section of the vertebral column at 3 wpf showing that *ctsk*:mEGFP-expressing cells at the neural and haemal arches (E) are TRAP positive (F).

scales (data not shown). Identical patterns were observed in independently generated transgenic lines using the same *ctsk* promoter to drive expression of cytoplasmically localized mCherry (*ctsk*:mcherry; Fig. 4I,J; supplementary material Fig. S6).

Characterization of medaka *rankl*

The full-length open reading frame (ORF) of medaka *rankl* encodes a deduced protein of 261 amino acids. It contains a tumour necrosis factor (TNF) superfamily domain (amino acids 100-256) that shares 35% identity and 48% similarity with its orthologue in humans (Fig. 3A). A PCR using primers flanking start and stop codons (supplementary material Fig. S3) and cDNA derived from 1-month-old wild-type fish resulted in three distinct fragments. Sequence analysis revealed three alternatively spliced isoforms of *rankl* cDNA (*rankl1*, *rankl2* and *rankl3*) encompassing 786, 378 and 322 nucleotides, respectively. Using isoform specific primers, we confirmed that hatchlings and 1-month-old fish express all three identified *rankl* isoforms (supplementary material Fig. S2F). Alignment of these isoforms is shown in supplementary material Fig. S3. When compared with known *rankl* isoforms (Ikeda et al., 2001), these sequences suggest similar splicing patterns of *rankl* transcripts in mouse and medaka, as depicted in Fig. 3B,C, except that the ORFs in medaka are significantly shorter compared with mouse (261/125/59 amino acids compared with 316/287/199 amino acids). Interestingly, medaka isoforms 2 and 3, as well as mouse isoform 3 lack a predicted transmembrane domain.
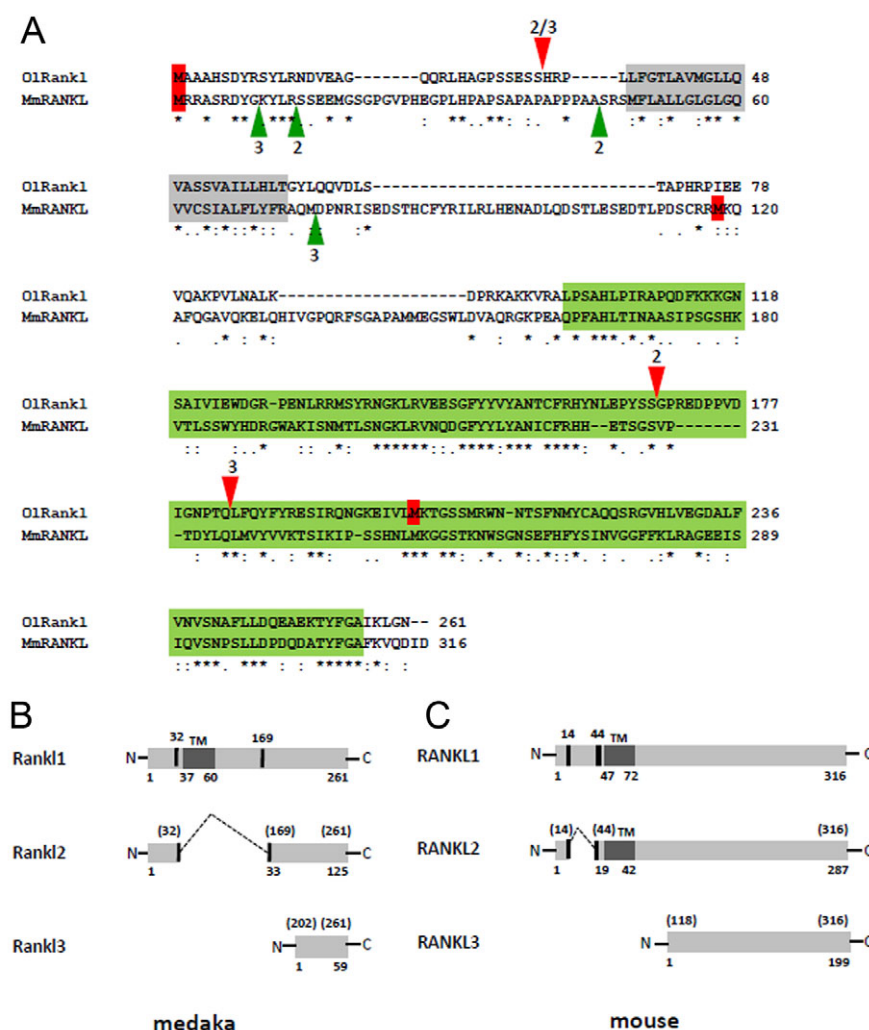
Fig. 3. Three alternatively spliced *rankl* isoforms in medaka (OlRankl) and mouse (MmRankl). (**A**) Amino acid alignment. Grey box indicates transmembrane domain, green box marks extracellular tumour necrosis factor (TNF) homology domain. Predicted translational start sites are in red. Arrowheads indicate alternative splice sites for isoforms 2 and 3. Isoform 1 is the full-length protein. (**B**) Three medaka Rankl isoforms predicted from obtained cDNA sequences. (**C**) Mouse Rankl isoforms as reported by Ikeda et al. (Ikeda et al., 2001).

Generation of transgenic medaka with inducible Rankl expression

We next generated *rankl*:HSE:CFP transgenic medaka lines carrying a bidirectional heat-shock inducible promoter that allows simultaneous expression of Rankl and CFP after incubating embryos at 39°C for 2 hours (supplementary material Fig. S2). To determine the efficiency of induction, we heat-shocked *rankl*:HSE:CFP embryos at different stages for 2 hours at 39°C (supplementary material Fig. S2). After heat-shock, expression levels of *rankl* were analysed by RNA in situ hybridization and RT-PCR. Both CFP and *rankl* were found to be expressed ubiquitously at high levels in transgenic embryos at different stages (supplementary material Fig. S2). Ectopic *rankl* expression was observed at 3 and 12 dpf, 2 and 3 days after heat-shock, respectively, by in situ hybridization and semi-quantitative RT-PCR. This confirms that the used heat-shock conditions can induce ectopic *rankl* expression and that CFP serves as a suitable reporter co-expressed with *rankl* for early screening.

Formation, morphology and activities of Rankl-induced osteoclasts

We crossed *rankl*:HSE:CFP with *ctsk*:mEGFP fish to generate double transgenic lines overexpressing Rankl after heat-shock induction. *ctsk*:mEGFP sibling embryos served as controls. Embryos of both control and experimental groups were heat-shocked at 9 dpf. As described above, *ctsk*:mEGFP control embryos did not show GFP expression at the vertebral centra at this stage (Fig. 1L; also see Fig. 6A). By contrast, double transgenic *rankl*:HSE:CFP/*ctsk*:mEFP embryos showed the appearance of several mEGFP-positive cells in the vertebral column as described in detail below (see Fig. 6B,D). We used confocal time lapse imaging to observe origin, division, morphology and motility of these Rankl-induced ectopic osteoclasts. Living embryos were stained with Alizarin Complexone to visualize mineralized centrum structures in vivo and time-lapse imaging was started 1 day after heat-shock induction (supplementary material Movies 1, 2). Fig. 4A-H shows representative images at selected time points over a period of 20 hours. Most notably, first mEGFP labelled osteoclasts were observed in the intervertebral regions (Fig. 4, arrowhead in A, white arrow in E). Shortly after their appearance, these cells directly moved towards the centra and became closely associated with the mineralized matrix of vertebral bodies as well as haemal and neural arches (Fig. 4; 29/29 analysed cells in four embryos; arrowheads in B-H; white and purple arrows in F-H, blue and yellow arrows in G,H). During their migration, several cells underwent cell division (Fig. 4, arrowhead in D, white arrow in F). Upon reaching the mineralized matrix, the cells started to grow dynamic processes, which is a typical hallmark of osteoclasts in mammals (Chambers, 2010). We also performed heat-shock at later stages, i.e. at 21 and 23 dpf, when endogenous osteoclasts are
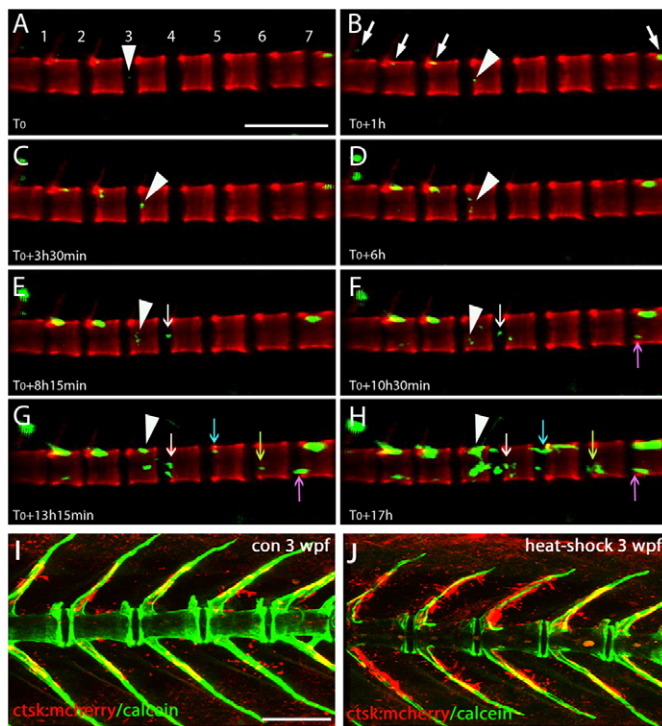
Fig. 4. Origin and migratory behaviour of Rankl-induced osteoclasts. Images are taken from a 20-hour time lapse confocal movie of *rankl*:HSE:CFP-*ctsk*:mEGFP double transgenic larvae at 10 dpf, 1 day after heat-shock (see supplementary material Movie 1). Mineralized matrix is stained in red. Intervertebral regions are numbered. Arrows follow newly formed individual osteoclasts over time. (**A**) The first induced osteoclast appears in intervertebral region 3 (arrowhead). (**B-E**) It migrates towards the mineralized vertebral body, pauses and undergoes cell division (D,E). (**F-H**) Both daughter cells move towards the neural and haemal arches (arrowheads in subsequent panels). Additional osteoclasts appear in other intervertebral regions (indicated by coloured arrows), undergo division and migrate towards mineralized vertebral bodies. (**I,J**) Osteoclast formation after heat-shock at 3 wpf in *rankl*:HSE:CFP-*ctsk*:mcherry larvae. Mineralized matrix is stained with calcein (green). Arrows in B indicate osteoclasts at the base of neural arches that either originated from cells in the intervertebral region or were born at the arches. Control (con) is a double-transgenic larva without heat-shock. Scale bars: 100 µm in A; 200 µm in I.

already present. This also resulted in a drastic increase in the number of *ctsk*:mcherry-expressing cells that were located not only at the inside of neural and haemal arches as in controls, but also on the outside of these skeletal elements (Fig. 4I,J).

The Rankl-induced cells showed irregular shapes and sizes ranging from 20-50 µm, with or without protrusions, depending on their stage of differentiation (Fig. 5B′-D′). At early differentiation stages, osteoclasts had an overall length of about 20-25 µm with an elongated shape lacking any protrusions (Fig. 5B′). One day later, these cells became flat, larger in size (40-50 µm) and developed dynamically growing protrusions (Fig. 5C′). On day 3, the cells continued to form new protrusions but remained flat in shape (Fig. 5D′). At later stages, several osteoclasts were observed to form clusters with close contact to each other and the mineralized matrix, making it difficult to distinguish and count individual cells (Fig. 5E,F).

A characteristic feature of mammalian osteoclasts is that they are multinucleated. By contrast, osteoclasts in advanced teleost fish such as medaka are typically mononucleated (Witten and Huysseune, 2009). We therefore examined the number of nuclei in Rankl-induced osteoclasts using nuclear DRAQ5 staining on cryosections. This revealed that all mEGFP cells analysed contained single nuclei (Fig. 5G,H). In addition, we found no evidence for any ruffled border, as typically seen in mammalian osteoclasts. However, several vacuoles were visible close to the surface membrane adjacent to the mineralized matrix of the neural arches (Fig. 5H).

Life imaging of dynamic interactions between osteoblasts and Rankl-induced osteoclasts

Interactions between osteoclasts and osteoblasts occur during all phases of bone remodelling in mammals (Matsuo and Irie, 2008). Communication between these cell types is essential for osteoclast formation and for controlled osteoblast activities. We took confocal pictures of Rankl-induced osteoclasts at 1, 2 and 3 days after their appearance in triple transgenic embryos that additionally express mCherry in osteoblasts under control of the *osterix* promoter (*rankl*:HS:CFP/*ctsk*:mEFP/*osx*:mcherry; Fig. 5A-D). As reported earlier, *osx*:mcherry expressing osteoblasts are present at all haemal and neural arches of the vertebral column at 9-12 dpf (Fig. 5A) (Renn and Winkler, 2009). After heat-shock at 9 dpf, we observed that the vast majority of mEGFP-labelled osteoclasts were in close contact with mCherry expressing osteoblasts (Fig. 5A-D). Time-lapse analysis revealed that these osteoclasts are highly dynamic, extend and retract large protrusions, and migrate towards osteoblasts (supplementary material Fig. S5, Movie 3). After Rankl-induced osteoclasts had formed in the intervertebral regions and started to express GFP, they directly approached the mineralized notochordal sheath. Once they reached this matrix, they ceased migration and quickly associated with osteoblasts to undergo further morphological differentiation. Osteoclasts that made tight contact with osteoblasts appeared immobilized, remained in the vicinity of osteoblasts but continued to dynamically extend their protrusions. After heat shock, we also observed frequent cell death both in Rankl-induced cells that failed to establish osteoblast contact and in those that were in tight connection to osteoblasts. Movies 3 and 5 (supplementary material) show the tight contact established between osteoclasts and osteoblasts.

Ectopic Rankl expression induces a severe osteoporosis-like phenotype

One to two days after heat-shock-induced Rankl expression, we observed strong mEGFP expression in the vertebral column of embryos overexpressing Rankl (Fig. 6B). Confocal stacks of images of the mineralized vertebral column stained by Alizarin Complexone showed that ectopic *ctsk*:mEGFP cells were closely attached to the mineralized matrix of neural and haemal arches, and also with the centra of the vertebral bodies (Fig. 6C,D). RNA in situ hybridization and histochemistry for osteoclast markers *cathepsin K* and TRAP, respectively, showed that cells expressing mEGFP were positive for both markers (Fig. 6E-H), strongly suggesting that Rankl-induced *ctsk*:mEGFP cells are functional osteoclasts. This prompted us to examine bone and centra mineralization in embryos at 16 dpf, 7 days after Rankl induction. Alizarin Red staining revealed a degradation of mineralized matrix, reflecting a mild osteoporosis-like phenotype. Bone matrix degeneration was most evident in neural and haemal arches (Fig. 6I,J). In some embryos, loss of mineralization also affected vertebral bodies (data not shown).
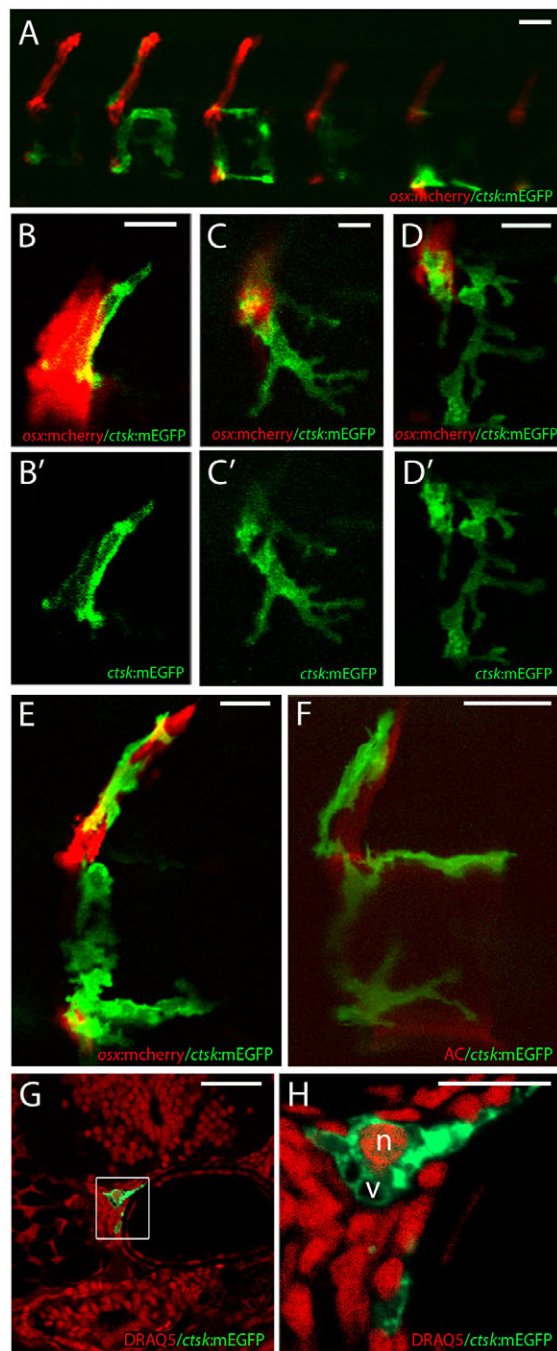
Fig. 5. Osteoclast-osteoblast interaction analysed in triple transgenic *rankl*:HSE:CFP/*ctsk*:mEGFP/*osx*:mcherry larvae.
(**A**) Confocal stack showing a region of the vertebral column after Rankl induction. (**B-D**) Confocal images of a *ctsk*:mEGFP-expressing osteoclast in direct contact with *osx*:mcherry-positive osteoblasts around a neural arch at day 1-3 after its appearance in triple transgenic larva. (**B'-D'**) As B-D but only GFP images are shown to demonstrate changes in morphology. (**E**) Osteoclast cluster in tight contact with osteoblasts. (**F**) Osteoclast cluster tightly associated with mineralized matrix stained with Alizarin Complexone (red). (**G**) Nuclear staining with DRAQ5 (633 nm; red) on cryosection through vertebral column reveals osteoclast associated with the base of the neural arch. (**H**) Higher magnification of the osteoclast boxed in G, showing that cell has one nucleus (n) and no ruffled border, but several vacuoles (v), close to the membrane adjacent to the neural arch. Scale bars: 10 μm, except in A and G (30 μm).

To test whether mEGFP expression has any effect on the activity of Rankl-induced osteoclasts and hence the severity of mineralization loss, we next analysed the effect of Rankl induction on mineralization of bone and the notochordal sheath in *rankl*:HSE:CFP single transgenic embryos. After heat-shock at 9 dpf, mineralization was analysed at 16 dpf by Alizarin Red staining. Even though both heterozygous single *rankl*:HSE:CFP transgenics and *rankl*:HSE:CFP/*ctsk*:mEGFP double transgenic larvae were derived from the same *rankl*:HSE:CFP founder, we observed striking differences in the effects on mineralized matrix. Single transgenic *rankl*:HSE:CFP larvae showed a much stronger loss of mineralization than did double transgenic larvae after induction of Rankl expression. It is unclear why the severity of this osteoporosis-like phenotype varies between both fish lines, but we suspect that transgenic expression of membrane-tethered EGFP might interfere with the activity of mEGFP-labelled osteoclasts.

In single transgenic *rankl*:HSE:CFP larvae, we observed a severe loss in mineralized matrix of most embryos overexpressing Rankl; however, these losses varied in extent (Fig. 7A,B). Loss of mineralization was observed in skeletal structures of the head and the tail, and most obviously in the centra of the vertebral bodies, while interestingly mineralization in the pharyngeal teeth region was not affected. In the axial skeleton at 16 dpf, wild-type fish after heat-shock showed strong Alizarin Red staining in the vertebral bodies consisting of the mineralized centrum and the neural as well as haemal arches (Fig. 7C). In embryos overexpressing Rankl, arches were almost completely absent and we observed severe damage in the mineralized matrix of the vertebral centra (Fig. 7D). Moreover, we observed substantial disorganization in the notochord of Rankl-overexpressing embryos. At 11 dpf, i.e. 2 days after the heat-shock, histological analysis revealed an intact notochord with large vacuolated cells and a thin peripheral notochord epithelium (Fig. 7E). At 12 dpf, however, we observed a pronounced increase in cells that had the appearance of notochordoblasts and occupied the central part of the notochord (Fig. 7F). At 13 dpf, more small vacuolated cells appeared and the notochord epithelium became highly disorganized (Fig. 7G). At 16 dpf, the centra of the vertebral bodies had almost completely lost their mineralized notochordal sheath as well as the surrounding elastin layer at the base of the arches (Fig. 7I), whereas these structures were fully intact in control embryos after heat-shock (Fig. 7H). Thus, although in control samples, large vacuolated notochord cells were aligned in a highly organized manner, the notochord cells in Rankl-overexpressing larvae showed variable sizes and randomly organized arrangement. Most importantly, we observed the appearance of large clusters of small cells in the middle of the notochord, which are normally found exclusively at the periphery of the notochord. In addition, heat-shock at 3 wpf, when endogenous osteoclasts are already active, resulted in substantial mineralization defects (supplementary material Fig. S8).

DISCUSSION

In the present study, we generated stable medaka transgenic lines to visualize osteoclast activation, osteoclast-osteoblast interaction and bone resorption. We were able to dissect conserved and divergent features of osteoclastogenesis and bone resorption induced by Rankl in the teleost fish medaka. Double transgenic reporter lines expressing mEGFP under control of the *cathepsin K* promoter (*ctsk*:mEGFP) and mCherry under control of the *osterix* promoter allowed visualization of osteoclast and osteoblast interaction in vivo. Overexpression of Rankl in the *rankl*:HSE:CFP line resulted in a strong osteoporosis-like phenotype with severe
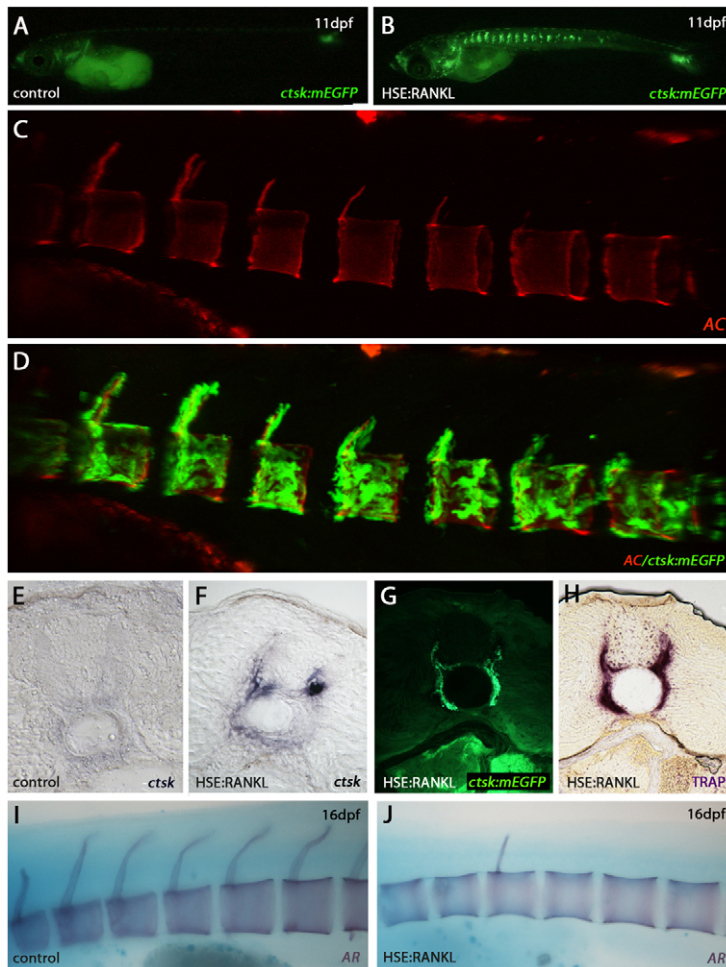
Fig. 6. Rankl overexpression induces functional ectopic osteoclasts and osteoporotic phenotype. HSE:Rankl, embryo overexpressing Rankl. (**A**) *ctsk*:mEGFP control embryo at 11 dpf, 2 days after heat shock. There is no GFP in the trunk. (**B**) *rankl*:HSE:CFP/*ctsk*:mEGFP double transgenic embryo at 11 dpf with strong ectopic *ctsk*:mEGFP expression in the vertebral column after heat shock. (**C**) Confocal image of the vertebral column stained with Alizarin Complexone in a double transgenic embryo 2 days after heat-shock. (**D**) Same image as in C but with both red and green channels to show ectopic *ctsk*:mEGFP expression in the mineralized vertebral column. (**E,F**) In situ hybridization for *cathepsin K* on transverse cryosections of a control (E) and Rankl-overexpressing (F) embryo. (**G,H**) TRAP staining on adjacent cryosection with ectopic osteoclasts in green (G) of a double transgenic embryo showing that mEGFP cells are positive for TRAP (H). (**I,J**) Alizarin Red staining of control embryo (I) and Rankl-overexpressing embryo (J) showing reduced mineralization of the neural arches after Rankl overexpression.

degradation of newly mineralized matrix in the vertebral column and other bone structures. To the best of our knowledge, this is the first report on real-time non-invasive visualization of Rankl-induced osteoclasts and their interaction with osteoblasts in vivo. This model will be an attractive tool for the osteoporosis research community, e.g. for chemical and genetic screenings.

cathepsin K expression in teleost fish

Ctsk is a lysosomal cysteine protease essential for osteoclast function and activity (Saftig et al., 2000). Both Ctsk as well TRAP are the most commonly used markers for osteoclasts in mammals and TRAP has been validated as osteoclast marker for fish in several studies (reviewed by Witten and Huysseune. 2009). In this study, we showed that mEGFP expression under the control of a 3.18 kb *ctsk* regulatory region recapitulated most of the endogenous *ctsk* expression patterns. Interestingly, endogenous *ctsk* expression in heart, individual brain neurons and pineal gland was not found in the transgenics, suggesting that the used promoter lacks regulatory elements driving expression in these non-skeletal tissues. Around 5 dpf, first endogenous as well as transgenic expression was found in the mesenchyme of the head and developing fins. At this stage, bone has not yet been formed, and we think it is unlikely that these cells become osteoclasts as they are and remain TRAP negative in this region (data not shown). We speculate that these cells are involved in remodelling extracellular matrix as this mesenchyme is transformed into muscle at later stages. First *ctsk*:mEGFP expression in TRAP-positive cells was observed in pharyngeal replacement teeth and their supporting bones at 12 dpf, indicating that these are the first functional osteoclasts formed. It has been reported for fish and other non-mammalian vertebrates, that teeth are replaced throughout life (Van der heyden et al., 2000). The presence of osteoclasts therefore is indicative for bone remodelling associated with tooth replacement. This is consistent with previous reports that multi- and mononucleated osteoclasts found in the pharyngeal regions are related to shedding teeth and their supporting bone (Nemoto et al., 2007; Witten, 1997). In the vertebral column, *ctsk*:mEGFP and endogenous *ctsk* expression was first observed three to four weeks after fertilization in cells attached to the neural and haemal arches. These cells are TRAP positive, indicating that they are functional osteoclasts, which is consistent with previous histological reports on flat mononuclear TRAP-positive osteoclasts without ruffled border found along the vertebral column of zebrafish (Witten et al., 2001) and medaka (Nemoto et al., 2007). Neural and haemal arches enclose the spinal cord and the dorsal aorta, respectively, and osteoclasts are required for bone remodelling in this region to provide extending space for the rapidly growing spinal cord and blood vessel. We found that the osteoclasts were motile with dynamic protrusions and arranged in clusters indicative for intense bone resorption activities (Witten, 1997). By contrast, the centra of the teleost vertebral bodies form after mineralization of the notochordal sheath and subsequent apposition of bone matrix, without the need for bone resorption (reviewed by Witten and Huysseune, 2009). Therefore, no osteoclasts are present around the centra.
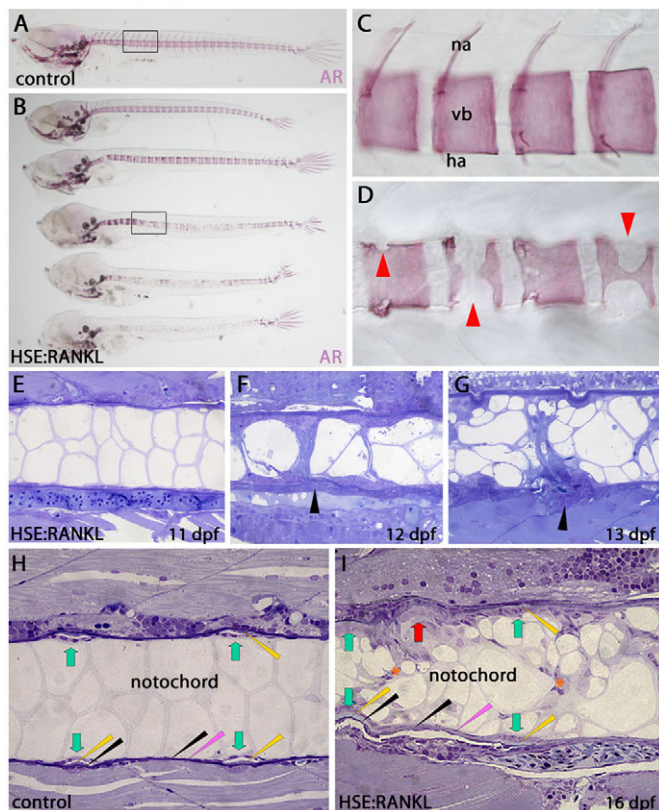
Fig. 7. Severe osteoporosis-like phenotype in *rankl*:HSE:CFP transgenic medaka overexpressing Rankl at 16 dpf, 7 days after heat shock. (**A**) Alizarin Red stained control fish shows intact mineralization in head, vertebral column and tail. (**B**) Transgenic fish overexpressing Rankl show severely damaged mineralized structures. (**C,D**) High magnification view of regions boxed in A,B reveals loss of mineralized matrix in neural arches and vertebral bodies of larva overexpressing Rankl (red arrowheads; D) compared with control (C). (**E-I**) Sagittal 1 μm epon sections through vertebral column of Rankl-overexpressing larvae at 11, 12, 13 and 16 dpf (E-G,I) and 16 dpf control (H) stained with Toluidine Blue. Intact vertebral body wall consists of mineralized notochordal sheath (pink arrowheads) covered by an elastin layer (slim black arrowheads in H,I). Green arrows indicate position of prospective intervertebral discs. These areas are severely damaged in Rankl larvae (red arrow in I) that lack most of the mineralized notochordal sheath and elastin layer. The number of small cells increases starting from 12 dpf inside the notochord of Rankl samples (orange asterisks in I). Yellow arrowheads indicate thickened non-mineralized notochord sheath in the intervertebral space. Arrowheads in F,G indicate fenestration of the notochordal sheath.

Morphology of Rankl-induced osteoclasts

In contrast to the typically multinucleated mammalian osteoclasts, Rankl-induced osteoclasts in medaka were found to be mononucleated, although we do not exclude that they become multinucleated at later stages. They also did not exhibit a ruffled border but contained large vacuoles close to the membrane adjacent to the mineralized matrix. Our data on osteoclast morphology are consistent with histological data reported previously. Witten et al. (Witten et al., 2001) described mononucleated osteoclasts at the inner side of neural arches in zebrafish, and Nemoto et al. (Nemoto et al., 2007) made similar observations in medaka. Mononucleated osteoclasts were described in most teleost fish species with acellular bone such as medaka. A link between acellular bone and

the predominance of mononucleated osteoclasts in contrast to cellular bone and multinucleated osteoclasts has been suggested (Witten and Huysseune, 2009). Multi- and mononucleated osteoclasts differ in their morphology, as well as in the mode of bone resorption. Mononucleated osteoclasts lack a ruffled border and may not exhibit resorption lacunae. They instead form cell aggregates resembling multinucleated giant cells in mammals during intense bone resorption (Witten, 1997; Witten and Huysseune, 2009). Although osteoclasts are generally assumed to be multinucleated in mammals, cell counting revealed that 30-50% of active human osteoclasts are mononucleated (Chambers, 1985; Evans et al., 1979; Kaye, 1984). According to Parfitt (Parfitt, 1988) multinucleated osteoclasts are responsible for fast and deep bone resorption, whereas mononucleated osteoclasts resorb smaller amounts of bone. It is, thus, interesting that overactivated osteoclasts in medaka that cause a severe osteoporotic phenotype are still mononucleated. Moving away from the paradigm that only multinucleated osteoclasts resorb bone may help to acknowledge the role of mononucleated osteoclasts in mammals and their possible involvement in bone loss.

Rankl overexpression in medaka results in an osteoporotic phenotype

After heat-shock induction, *rankl*:HSE:CFP transgenic larvae showed a strong osteoporosis-like phenotype at 16 dpf, 7 days after the heat-shock. Newly mineralized matrix in different skeletal structures of the embryos was damaged to different extent, most obvious in the neural and haemal arches, vertebral bodies and the mineralized notochordal sheath. Almost no matrix was left in the arches, which may reflect the fact that these are the first sites of newly formed bone in the trunk. The osteoporosis-like phenotype was caused by functional ectopic osteoclasts, as revealed in double transgenic *rankl*:HSE:CFP/*ctsk*:mEGFP larvae. This effect seemed to be dose dependent on ectopic Rankl as the severity varied in offspring from different founders, with a clear correlation to CFP expression (data not shown).

In mammals, Rankl is expressed by osteoblasts and stromal cells and is known as the major osteoclast differentiation factor (Kong et al., 1999; Lacey et al., 1998). It promotes osteoclastogenesis and maintains bone homeostasis through binding to its receptor RANK, modulated by osteoprotegerin (OPG) (Anderson et al., 1997; Simonet et al., 1997; Yasuda et al., 1999). The RANK receptor is expressed by osteoclast progenitors, whereas OPG acts as a decoy receptor for Rankl and thereby controls the number of osteoclasts formed.

In human and mouse, three alternatively spliced isoforms of Rankl are capable of promoting osteoclastogenesis (Ikeda et al., 2001; Suzuki et al., 2004). Two of these isoforms are type II transmembrane glycoproteins that ensure cell-cell contact with osteoclasts and their precursors. The third isoform lacks transmembrane and intracellular domains and acts as soluble ligand (sRankl) allowing diffusion to activate target cells (Ikeda et al., 2001; reviewed by Wright et al., 2009). Mice overexpressing soluble or membrane bound forms of Rankl ubiquitously, die after E18.5 due to unknown reasons (Mizuno et al., 2002). During embryogenesis, the bones of these mice form normally; however, they exhibit mildly reduced calcification. Mice that overexpress Rankl exclusively in the liver, however, are viable and develop severe late onset osteoporosis (Mizuno et al., 2002).

In our transgenic approach, Rankl was overexpressed ubiquitously after heat-shock treatment on day 9. The cDNAs identified in medaka presumably give rise to one full-length

membrane bound Rankl isoform as well as two shorter soluble variants (Fig. 3B; supplementary material Fig. 2F). Other than in mammals, where the TNF domain is present in all three isoforms, only medaka isoform 1 contains a complete TNF domain, whereas isoforms 2 and 3 include only parts. It will be interesting to test whether the three medaka isoforms have similar osteoclastogenic activities and whether these differences have any evolutionary significance. Nevertheless, the strong osteoporosis-like phenotype observed in this study upon Rankl induction suggests a conserved role of Rankl for osteoclastogenesis in medaka.

A significant re-organization of notochordal cells was observed in embryos overexpressing Rankl that exhibited severe degradation of the mineralized matrix in the vertebral bodies. Further work is required to determine the exact identity of these cells. We speculate, however, that this could reflect a compensatory mechanism where the notochord responds to damage of the notochordal sheath. The notochord has previously been implemented in the formation of vertebral bodies in zebrafish and Atlantic salmon (Fleming et al., 2004; Grotmol et al., 2005) and our osteoporotic model may help to gain insight into the role that the notochord plays in vertebral body formation.

The origin of Rankl-induced osteoclasts

Our transgenic approach allowed us to monitor the birth, migration and differentiation of Rankl-induced osteoclasts in living embryos and to study their interactions with osteoblasts. Other than in earlier studies using mouse models (Mizuno et al., 2002), Rankl expression in our model was temporally controlled and induced at a stage when bone mineralization was well under way. In *rankl*:HSE:CFP/*ctsk*:mEGFP double transgenic embryos, ectopic osteoclasts could only be observed after 7 dpf, regardless of how early Rankl misexpression had been induced (data not shown). This suggests that before this stage any precursor cells present are not competent to respond to Rankl, possibly because Rank receptor expression has not been initiated. Interestingly, Rankl-induced ectopic osteoclasts in the vertebral bodies form long before the first endogenous osteoclasts become visible in the neural and haemal arches. The vast majority of these pioneering osteoclasts were interestingly found to originate in the intervertebral regions.

In mammals, macrophages and osteoclasts share common precursor cells of the hematopoietic/macrophage lineage in the bone marrow. The fate of either cell type is determined by local factors inhibiting differentiation of the other (Mann et al., 2010). As teleost fish lack hematopoietic bone marrow tissue, the hematopoietic equivalent is located in the head kidney (pronephros) but the origin of osteoclasts is still unknown (Apschner et al., 2011). The first Rankl-induced osteoclasts were observed in intervertebral regions, i.e. directly anterior to the segmental blood vessels and dorsal to the aorta. The determination of the cell lineage of Rankl-induced mononucleated osteoclasts remains unclear. However, expression of indicative markers such as TRAP and cathepsin K, as well as their activation by Rankl, makes it likely that the induced cells in medaka share the same hematopoietic origin as mammalian osteoclasts. Interestingly, there is recent evidence in mice for the presence of cycle-arrested quiescent osteoclast precursors (QOPs) that circulate in peripheral blood (Muto et al., 2011). We found *rank*-expressing cells in the dorsal aorta, as well as around the notochord in Rankl-induced fish (supplementary material Fig. S4). Assuming that normal *rank* expression occurs at the same location as evidenced after heat-shock treatment, it will be interesting to test whether, in teleost fish, Rankl-induced *ctsk*-positive osteoclasts differentiate from QOPs

circulating in surrounding blood vessels, or alternatively are derived from the monocyte/macrophage lineage. The transgenic lines presented here will be valuable tools to address this important issue.

Competing interests statement
The authors declare no competing financial interests.

Supplementary material
Supplementary material available online at
http://dev.biologists.org/lookup/suppl/doi:10.1242/dev.071035/-/DC1

References
Anderson, D. M., Maraskovsky, E., Billingsley, W. L., Dougall, W. C., Tometsko, M. E., Roux, E. R., Teepe, M. C., DuBose, R. F., Cosman, D. and Galibert, L. (1997). A homologue of the TNF receptor and its ligand enhance T-cell growth and dendritic-cell function. *Nature* **390**, 175-179.

Apschner, A., Schulte-Merker, S. and Witten, P. E. (2011). Not all bones are created equal-using zebrafish and other teleost species in osteogenesis research. *Methods Cell Biol.* **105**, 239-255.

Bajoghli, B., Aghaallaei, N., Heimbucher, T. and Czerny, T. (2004). An artificial promoter construct for heat-inducible misexpression during fish embryogenesis. *Dev. Biol.* **271**, 416-430.

Caetano-Lopes, J., Canhao, H. and Fonseca, J. E. (2007). Osteoblasts and bone formation. *Acta Reumatol. Port.* **32**, 103-110.

Chambers, T. J. (1985). The pathology of the osteoclast. *J. Clin. Pathol.* **38**, 241-252.

Chambers, T. J. (2010). The birth of the osteoclast. *Ann. New York Acad. Sci.* **1192**, 19-26.

Chatani, M., Takano, Y. and Kudo, A. (2011). Osteoclasts in bone modeling, as revealed by in vivo imaging, are essential for organogenesis in fish. *Dev Biol*. (in press).

Evans, R. A., Dunstan, C. R. and Baylink, D. J. (1979). Histochemical identification of osteoclasts in undecalcified sections of human bone. *Miner. Electrolyte Metab.* **2**, 179-185.

Fleming, A., Keynes, R. and Tannahill, D. (2004). A central role for the notochord in vertebral patterning. *Development* **131**, 873-880.

Flores, M. V., Tsang, V. W., Hu, W., Kalev-Zylinska, M., Postlethwait, J., Crosier, P., Crosier, K. and Fisher, S. (2004). Duplicate zebrafish runx2 orthologues are expressed in developing skeletal elements. *Gene Expr. Patterns* **4**, 573-581.

Gallagher, J. C. and Sai, A. J. (2010). Molecular biology of bone remodeling: Implications for new therapeutic targets for osteoporosis. *Maturitas* **65**, 301-307.

Grotmol, S., Nordvik, K., Kryvi, H. and Totland, G. K. (2005). A segmental pattern of alkaline phosphatase activity within the notochord coincides with the initial formation of the vertebral bodies. *J. Anat.* **206**, 427-436.

Hammond, C. L. and Schulte-Merker, S. (2009). Two populations of endochondral osteoblasts with differential sensitivity to Hedgehog signalling. *Development* **136**, 3991-4000.

Harada, S. and Rodan, G. A. (2003). Control of osteoblast function and regulation of bone mass. *Nature* **423**, 349-355.

Ikeda, T., Kasai, M., Utsuyama, M. and Hirokawa, K. (2001). Determination of three isoforms of the receptor activator of nuclear factor-kappaB ligand and their differential expression in bone and thymus. *Endocrinology* **142**, 1419-1426.

Inohaya, K., Takano, Y. and Kudo, A. (2007). The teleost intervertebral region acts as a growth center of the centrum: In vivo visualization of osteoblasts and their progenitors in transgenic fish. *Dev. Dyn.* **236**, 3031-3046.

Inohaya, K., Takano, Y. and Kudo, A. (2010). Production of Wnt4b by floor plate cells is essential for the segmental patterning of the vertebral column in medaka. *Development* **137**, 1807-1813.

Karsenty, G. (2008). Transcriptional control of skeletogenesis. *Annu. Rev. Genomics Hum. Genet.* **9**, 183-196.

Kaye, M. W. (1984). When is it an osteoclast? *J. Clin. Pathol.* **37**, 398-400.

Komori, T. (2008). Regulation of bone development and maintenance by Runx2. *Front. Biosci.* **13**, 898-903.

DEVELOPMENT

Kong, Y. Y., Yoshida, H., Sarosi, I., Tan, H. L., Timms, E., Capparelli, C., Morony, S., Oliveira-dos-Santos, A. J., Van, G., Itie, A. et al. (1999). OPGL is a key regulator of osteoclastogenesis, lymphocyte development and lymph-node organogenesis. *Nature* **397**, 315-323.

Lacey, D. L., Timms, E., Tan, H. L., Kelley, M. J., Dunstan, C. R., Burgess, T., Elliott, R., Colombero, A., Elliott, G., Scully, S. et al. (1998). Osteoprotegerin ligand is a cytokine that regulates osteoclast differentiation and activation. *Cell* **93**, 165-176.

Langille, R. M. and Hall, B. K. (1988). Role of the neural crest in development of the cartilaginous cranial and visceral skeleton of the medaka, Oryzias latipes (Teleostei). *Anat. Embryol.* **177**, 297-305.

Mann, M., Barad, O., Agami, R., Geiger, B. and Hornstein, E. (2010). miRNA-based mechanism for the commitment of multipotent progenitors to a single cellular fate. *Proc. Natl. Acad. Sci. USA* **107**, 15804-15809.

Matsuo, K. and Irie, N. (2008). Osteoclast-osteoblast communication. *Arch. Biochem. Biophys.* **473**, 201-209.

Mizuno, A., Kanno, T., Hoshi, M., Shibata, O., Yano, K., Fujise, N., Kinosaki, M., Yamaguchi, K., Tsuda, E., Murakami, A. et al. (2002). Transgenic mice overexpressing soluble osteoclast differentiation factor (sODF) exhibit severe osteoporosis. *J. Bone Miner. Metab.* **20**, 337-344.

Muto, A., Mizoguchi, T., Udagawa, N., Ito, S., Kawahara, I., Abiko, Y., Arai, A., Harada, S., Kobayashi, Y., Nakamichi, Y. et al. (2011). Lineage-committed osteoclast precursors circulate in blood and settle down into bone. *J. Bone Miner. Res.* (in press).

Nemoto, Y., Higuchi, K., Baba, O., Kudo, A. and Takano, Y. (2007). Multinucleate osteoclasts in medaka as evidence of active bone remodeling. *Bone* **40**, 399-408.

Parfitt, A. M. (1988). Bone remodelling: relationship to amount and structure of bone and the pathogenesis and prevention of fractures. In *Osteoporosis, Etiology, Diagnosis and Management* (ed. B. L. Riggs and L. J. Melton), pp. 45-93. New York: Raven Press.

Reid, I. R. (2008). Anti-resorptive therapies for osteoporosis. *Semin. Cell Dev. Biol.* **19**, 473-478.

Rembold, M., Lahiri, K., Foulkes, N. S. and Wittbrodt, J. (2006). Transgenesis in fish: efficient selection of transgenic fish by co-injection with a fluorescent reporter construct. *Nat. Protocols* **1**, 1133-1139.

Renn, J. and Winkler, C. (2009). Osterix-mCherry transgenic medaka for in vivo imaging of bone formation. *Dev. Dyn.* **238**, 241-248.

Renn, J., Schaedel, M., Volff, J. N., Goerlich, R., Schartl, M. and Winkler, C. (2006). Dynamic expression of sparc precedes formation of skeletal elements in the Medaka (Oryzias latipes). *Gene* **372**, 208-218.

Saftig, P., Hunziker, E., Everts, V., Jones, S., Boyde, A., Wehmeyer, O., Suter, A. and von Figura, K. (2000). Functions of cathepsin K in bone resorption. Lessons from cathepsin K deficient mice. *Adv. Exp. Med. Biol.* **477**, 293-303.

Simonet, W. S., Lacey, D. L., Dunstan, C. R., Kelley, M., Chang, M. S., Luthy, R., Nguyen, H. Q., Wooden, S., Bennett, L., Boone, T. et al. (1997). Osteoprotegerin: A novel secreted protein involved in the regulation of bone density. *Cell* **89**, 309-319.

Spoorendonk, K. M., Peterson-Maduro, J., Renn, J., Trowe, T., Kranenbarg, S., Winkler, C. and Schulte-Merker, S. (2008). Retinoic acid and Cyp26b1 are critical regulators of osteogenesis in the axial skeleton. *Development* **135**, 3765-3774.

Suzuki, J., Ikeda, T., Kuroyama, H., Seki, S., Kasai, M., Utsuyama, M., Tatsumi, M., Uematsu, H. and Hirokawa, K. (2004). Regulation of osteoclastogenesis by three human RANKL isoforms expressed in NIH3T3 cells. *Biochem. Biophys. Res. Commun.* **314**, 1021-1027.

Van der heyden, C., Huysseune, A. and Sire, J. Y. (2000). Development and fine structure of pharyngeal replacement teeth in juvenile zebrafish (Danio rerio) (Teleostei, Cyprinidae). *Cell Tissue Res.* **302**, 205-219.

Wagner, E. F. and Karsenty, G. (2001). Genetic control of skeletal development. *Curr. Opin. Genet. Dev.* **11**, 527-532.

Witten, P. E. (1997). Enzyme histochemical characteristics of osteoblasts and mononucleated osteoclasts in a teleost fish with acellular bone (Oreochromis niloticus, Cichlidae). *Cell Tissue Res.* **287**, 591-599.

Witten, P. E. and Huysseune, A. (2009). A comparative view on mechanisms and functions of skeletal remodelling in teleost fish, with special emphasis on osteoclasts and their function. *Biol. Rev. Camb. Philos. Soc.* **84**, 315-346.

Witten, P. E., Hansen, A. and Hall, B. K. (2001). Features of mono- and multinucleated bone resorbing cells of the zebrafish Danio rerio and their contribution to skeletal development, remodeling, and growth. *J. Morphol.* **250**, 197-207.

Wright, H. L., McCarthy, H. S., Middleton, J. and Marshall, M. J. (2009). RANK, RANKL and osteoprotegerin in bone biology and disease. *Curr. Rev. Musculoskelet. Med.* **2**, 56-64.

Yan, Y. L., Willoughby, J., Liu, D., Crump, J. G., Wilson, C., Miller, C. T., Singer, A., Kimmel, C., Westerfield, M. and Postlethwait, J. H. (2005). A pair of Sox: distinct and overlapping functions of zebrafish sox9 co-orthologs in craniofacial and pectoral fin development. *Development* **132**, 1069-1083.

Yasuda, H., Shima, N., Nakagawa, N., Yamaguchi, K., Kinosaki, M., Goto, M., Mochizuki, S. I., Tsuda, E., Morinaga, T., Udagawa, N. et al. (1999). A novel molecular mechanism modulating osteoclast differentiation and function. *Bone* **25**, 109-113.